Wetlands Ecol Manage (2022) 30:647–673
https://doi.org/10.1007/s11273-022-09880-6

ORIGINAL PAPER

Holocene evolution of a floodplain wetland in the dryland piedmont of central-west Argentina

Adriana E. Mehl · Marcelo A. Zárate · Florencia R. Lorenzo

Received: 7 June 2021 / Accepted: 14 April 2022 / Published online: 7 May 2022

Abstract In arid central-west Argentina, South America, many wetlands have developed in association with rivers draining the Andean piedmont and are vital hotspots for resources. However, knowledge about their long-term evolution is generally scarce. The Bañados del Atuel wetland, a low gradient fluvio-aeolian plain linked to the Atuel-Diamante fluvial system, is analyzed to depict its geomorphological and sedimentological Holocene evolution. The study area comprises a fluvial fill terrace with fine-grained alluvial deposits (~ 4186–4419 cal years BP), deposited by a palaeodistributary fluvial system, that is covered by SW–NE oriented aeolian dune complexes. The present-day wetland, which developed after formation of the fill terrace, is characterized by: (1) a NW–SE oriented floodplain with distributary channels and fine-grained, massive to laminated deposits of low organic matter content, dated to 2755–2864 and 729–895 cal years BP, and includes SW–NE oriented dune systems and salt flat depressions; and (2) a transfer area with active headcutting channels, entrenched in the fill terrace, that connects the NW–SE oriented floodplain with (3) a saline endorheic depression (salt lake) with active deflation. The fill terrace distribution suggests much more extensive floodplain environments prior to the late Holocene; the present-day wetland is not older than the last 2–3 millennia and records a late Holocene trend of floodplain size reduction. Fluvial processes of avulsion were likely driven by mid and late Holocene El Niño Southern Oscillation (ENSO) events. Late Holocene arid conditions favoured aeolian dune formation and fluvio-aeolian interactions. Furthermore, anthropogenic river modifications, starting ~ 200 years ago, also have promoted severe changes in the Atuel-Diamante fluvial system, deepening the aridity in the wetland.

Keywords Late quaternary · Wetland landforms · Avulsions · Aeolian dunes · Fluvio–aeolian interactions · Anthropogenic impact

A. E. Mehl (✉) · M. A. Zárate
CONICET - Universidad Nacional de La Pampa, Instituto de Ciencias de la Tierra y Ambientales de La Pampa (INCITAP), 6300 Santa Rosa, La Pampa, Argentina
e-mail: adrianamehl@gmail.com; adrianamehl@conicet.gov.ar

M. A. Zárate
e-mail: mzarate@exactas.unlpam.edu.ar

A. E. Mehl · M. A. Zárate · F. R. Lorenzo
Facultad de Ciencias Exactas y Naturales, Departamento de Geología, Universidad Nacional de La Pampa, 6300 Santa Rosa, La Pampa, Argentina
e-mail: lorenzoflorr@gmail.com

Introduction

In recent decades, wetlands have been revalued as hotspots of biodiversity and hydrological regulators (Malvárez 1999), as well as suppliers of a wide range of ecosystem services that contribute to human well-being (Tooth et al. 2015a). However, at present, wetlands are under pressure because of climate change and anthropogenic impacts that affect their delicate equilibrium (Malvárez 1999; Junk et al. 2013). Wetlands occupy 5–7% of the Earth's surface (Junk et al. 2013) and are key components of many landscapes worldwide (Tooth et al. 2015a) but wetlands in drylands have been reported as disproportionately important in terms of biodiversity and other ecosystem services (Tooth et al. 2015b).

South America is described as the wettest continent on Earth with wetlands covering ~ 20% of the continental area; the largest wetlands are associated with large tropical river systems (i.e. the Amazon, Orinoco, and Paraguay–Paraná rivers) (Wittmann et al. 2015). Periodically or permanently waterlogged wetlands not directly associated with rivers also cover vast areas of the continent (i.e. glacier-fed wetlands, permanent lakes, and brackish to hypersaline wetlands in semiarid and arid regions) (Wittmann et al. 2015). As regards rivers and wetlands in the drylands of South America, little information was available in the early 2000s (Tooth 2000). In different locations of North America, Africa, Australia and the Middle East, most previous studies had aimed to understand the geomorphology and sedimentology of dryland rivers (e.g. hydraulic geometry, processes of erosion and deposition, arroyos and gullies formation) (Tooth 2000) and only later did knowledge more specifically related to wetlands in drylands start to emerge (Tooth and McCarthy 2007). Importance was also given to understanding the diversity of processes and landforms that characterizes fluvio–aeolian interactions in drylands at different scales of analysis, i.e. global, regional and local scales (Bullard and McTainsh 2003). When a global approach is considered, climate and topography are the main controls on fluvial systems; however, aeolian systems not only depend on suitable wind conditions but also on a suitable sediment supply and usually a lack of vegetation. At a local scale, aeolian–fluvial interactions in drylands can be observed in individual landforms (e.g. source/bordering dunes) and can imply both the fluvial supply of sediment to aeolian systems but also the removal of sediment (e.g. gully formation by water erosion). Nevertheless, although the body of knowledge about rivers, wetlands in drylands and fluvio–aeolian interactions has become increasingly robust in different regions worldwide, the scarcity of information in the drylands of southern South America still persists.

In Argentina, located in southern South America (Fig. 1a inset), wetlands occupy ~ 600,000 km^2 (~ 21.5%) of the territory (Benzaquén et al. 2017). Some wetlands are developed in arid fluvial contexts of the Andean piedmont of central-west Argentina. These piedmont rivers, seasonally fed by meltwater from the high Andes, are vital for ecosystems and the various agricultural oases where most of the population is concentrated. Consequently, due to irrigation, farming, urbanization, and hydropower needs, many fluvial systems have been profoundly modified, leading to a drastic deterioration of the associated piedmont wetlands, and eventually to their present reduction in size and even disappearance (Difrieri 1980; Torres and Zambrano 2000; Zárate et al. 2018). This is the case for the Atuel and Diamante rivers (~ 34° 30′ S) that supply water to the San Rafael-General Alvear oasis. Formerly, these rivers drained into a wetland known as Bañados del Atuel (Fig. 1a, b). The condition of the wetland has severely deteriorated; for example, through loss of channel connectivity, floodplain salinization-desiccation, deflation of sediments from the river channel, deterioration of water quality, and exotic vegetation encroachment (Unlpam 2012; Dornes et al. 2013, 2016; Zárate et al. 2018). Consequently, it is mostly inactive at present and has turned more into a desert setting owing to continuous and progressive desiccation (Zárate et al. 2018).

Several technical reports by governmental agencies (e.g. Urbiztondo 1974; Zárate et al. 2005; Unlpam 2012) have aimed to restore the Bañados del Atuel wetland. Recently, some other studies have addressed wetland hydrology with the aim of quantifying changes since the construction of major dams upstream (e.g. El Nihuil dam—Fig. 1a) in the mid-twentieth century (e.g. Dornes et al. 2016). Although general geological and geomorphological features—for instance, a fluvial terrace, active and inactive channels, dunes and deflation basins—have been reported (Urbiztondo 1974; Zárate et al. 2005), a key issue yet to be studied is the wetland's development over longer timescales (i.e. before the historical and more recent timescales). Hence, this work is intended to interpret the evolution of this major wetland in the drylands of southern South America by means of the analysis of landforms (e.g. morphology, areal

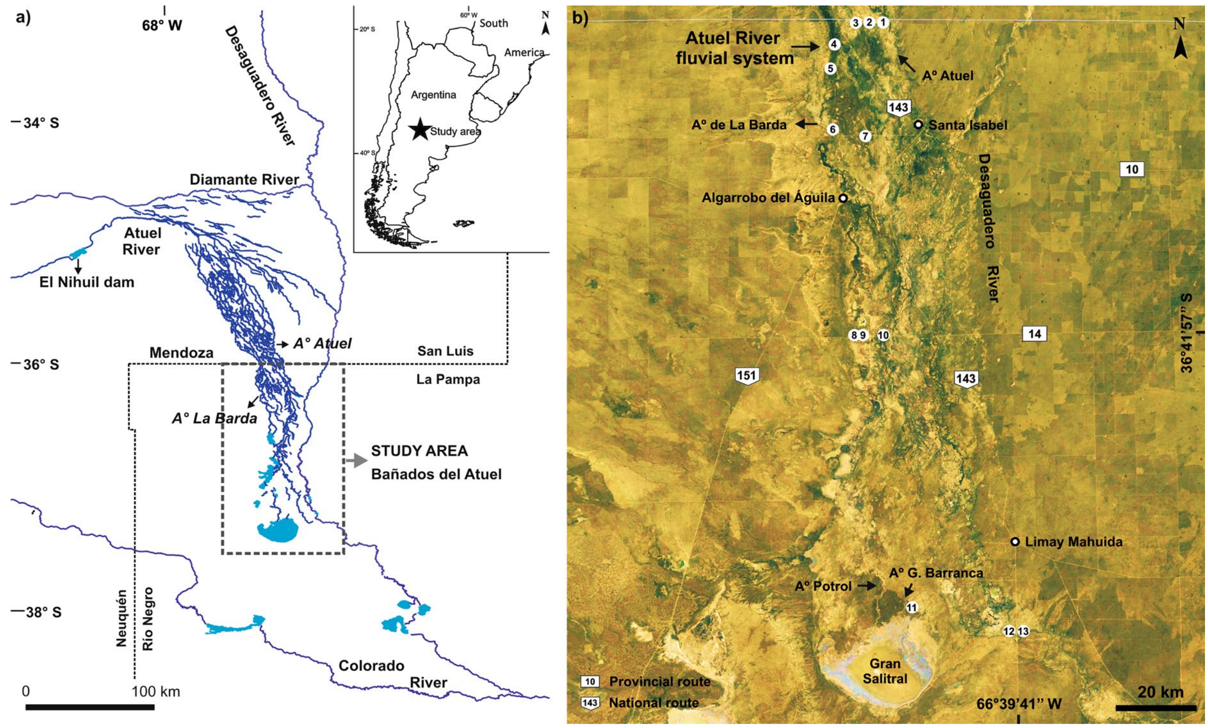

Fig. 1 Study area location: **a** Bañados del Atuel wetland in central-west Argentina region and main morphostructural/geomorphological units in the region (A° refers to arroyo); **b** detailed view of the study area (see box in a) and location of studied sedimentary Sections. 1 through 13: (1) 36º S I; (2) 36º S II; (3) 36º S III; (4) A° Barda 2; (5) A° Barda 1; (6) A° Barda 3; (7) A° Barda 4; (8) RP. 14 III; (9) RP. 14 II; (10) RP. 14 I; (11) Aº Gran Barranca; (12) Chadileuvú I; and (13) Chadileuvú II. Other numbers refer to provincial and national routes (see lower of image) (Google Earth © image capture)

distribution, geomorphological relationships) and key sedimentological sections. A chronological framework is proposed on the basis of radiocarbon dates and the correlation with stratigraphic records of surrounding areas. The results obtained indicate a mid to late Holocene development of the wetland. The main environmental and landscape changes can be linked to a climatic control, and in the last ~ 200 years to the anthropogenic impacts in the fluvial basin.

Environmental and geological setting

The Bañados del Atuel wetland lies in a dry, temperate region. Mean annual temperature is 15.6 °C with mean winter and summer temperatures of 7.2 °C and 23.7 °C, respectively (data from Santa Isabel locality—Fig. 1b). Mean annual rainfall (340 mm/year) is concentrated in the warmer season (September through March); the area is characterized by a great deficit in water balance owing to high evapotranspirative losses. The current wind regime (8–10 km/h average speed) in the study area is characterized by winds blowing dominantly from the N and the S along the year, with predominance of N winds during winter and S winds, with secondarily NE winds, in spring and summer (Cano 2004).

The Bañados del Atuel wetland has developed along the lower reach of the Atuel River, a tributary of the Desaguadero River (also known by local names, e.g. Salado, Chadileuvú, Curacó in La Pampa province, some of them of Christian origin and others of the native language—Cazenave 1979). The Desaguadero River is a N-S aligned trunk river that is a tributary of the Colorado River, the latter marking the boundary of the northern Patagonian region (Fig. 1a). The wetland has a shrinkage–expansion regime mainly linked to water inputs from the Atuel River (Dornes et al. 2016); it includes three main channels ("Butalo", "Atuel" and "de la Barda" arroyos, sensu

Urbiztondo 1974) and a reach of the Desaguadero River (Fig. 1).

The Atuel River is a perennial stream with a seasonal discharge regime that depends primarily on spring–summer melt of the winter snowfall over the high Andes Cordillera (Araneo and Compagnucci 2008). In the Central Andes (28º–36º S), interannual variations in precipitation, and consequently in snowmelt runoff volumes, are controlled by atmospheric circulation during the cold period of the year (Araneo and Villalba 2015). Above-average channel runoff related to abundant snowfall is associated with northward shifts in storm tracks caused by above-average sea surface temperatures in the equatorial Pacific (Araneo and Villalba 2015). Furthermore, extreme precipitation also occurs during some El Niño Southern Oscillation (ENSO) events, resulting in high discharges of the Atuel River (Araneo and Compagnucci 2008). The flooded area of the Bañados del Atuel wetland has reached more than 1600 km^2 during some of those extreme events; for example, in 1984 and 2007 (Dornes et al. 2016). In these extreme events, some of the main, largely inactive channels are occasionally reactivated (Zárate et al. 2005).

Geomorphologically, the wetland is partly characterized by distal playa environments located towards the tip of the Atuel River megafan (Fig. 1a–b) (Lorenzo 2019), the latter being bound by major faults (Criado Roqué and Ibáñez 1979). Southwards, the megafan is limited by the Neogene deposits of the Colorado River palaeofan (Fig. 1a–b). The wetland landscape is also characterized by isolated, low, rounded hills with flat surfaces composed of Late Proterozoic to Early Palaeozoic sedimentary, igneous and metamorphic rocks (Melchor and Casadío 2000; Melchor and Llambías 2004).

Materials and methods

The geomorphological features of the wetland study area were examined by remote sensing analysis based on open access satellite imagery; for instance, Landsat 5 and 8, and digital elevation models (e.g. TanDEM-X 90 m from the German Aerospace Center and MDE-Ar from the *Instituto Geográfico Nacional* of Argentina). Landform analysis (i.e. determination of topographic heights, slope gradients, fluvial stream sinuosity, and the distribution, length, width and orientation of other identified landforms) was assisted by free-access software (Google Earth, ENVI 5.00 free trial and QGis 2.14.2). Preliminary mapping of the study area was carried out; landscape units were identified and delimited. Then, landforms were selected for field surveys, including the checking and description of the geomorphic-geologic setting, the morphology, and the sedimentological characteristics. Analyzed sedimentary sections and pits were georeferenced and described following established sedimentological procedures and using standard criteria, i.e. sediment grain size, thickness, sedimentary structures, geometry and limits of the deposits (Tucker 2003). Colours were described with reference to the Munsell Soil Color Chart. Samples were collected for physico-chemical analysis and radiocarbon dating. Grain size analyses were conducted with a Malvern Mastersize Hydro 2000 laser diffractometer (2000–0.010 µm detection range) on pretreated (removal of organic matter, calcium carbonate and gypsum) and oven dried (< 60 °C) sediment samples. Grain size classification followed Folk's approach (1970). Total Organic Carbon (TOC) contents were determined by the loss on ignition technique (Heiri et al. 2001) and organic matter content derived from TOC by considering the Van Bemmelen factor (1.72) that assumes 58% of total organic carbon in soil organic matter. A digital calcimeter was used to determine calcium carbonate content.

Radiocarbon dates (Table 1) were obtained by Accelerator Mass Spectrometry (AMS) of organic matter and freshwater mollusc shells performed at the NFS Arizona AMS Facility laboratory (University of Arizona, USA). Calibration to calendar years (Table 1) with a 2 sigma range confidence interval (95.4%) was performed by means of CALIB 8.1.0 (Stuiver et al. 2021, at http://calib.org), and the SHCal20 Southern Hemisphere calibration dataset (Hogg et al. 2020).

Wetland landforms

The Bañados del Atuel wetland with an area of ~ 5500 km^2 (~ 200 km long N-S, ~ 40 km wide) is a low gradient (~ 0.55 m/km), fluvio-aeolian plain (Figs. 1b, 2) composed of fine-grained (sand, silt and mud) sediments. One of the most defining features is the occurrence of individual fluvial and aeolian landforms,

Table 1 ^{14}C AMS ages obtained in sedimentary deposits of the Bañados del Atuel wetland, lower reach of the Atuel River

Lithostratigraphic section	Sample depth	Laboratory N°	Material	$\delta^{13}C$	Uncalibrated age (^{14}C age BP)	Calibrated age 2Δ interval (cal. yrs BP)*
Aº Barda 3	~3.30 m	AA107927	OM in bulk sediment	– 25.6	3936 ± 23	4186–4195 (p: 0.009267)
						4235–4419 (p: 0.990733)
36º S II	~0.74 m	AA107929		– 23.5	914 ± 20	729–799 (p: 0.968198)
						871–879 (P: 0.02259)
						891–895 (p: 0.009212)
RP. 14 II	~0.45 m	AA109605		– 8.5	2746 ± 21	2755–2864 (p: 1)

*Calibration to calendar years with a 2 sigma confidence interval with the CALIB 8.1.0 (Stuiver, Reimer and Reimer Copyright 2021) and the SHCal20 Southern Hemisphere calibration dataset (Hogg et al. 2020). OM: organic matter

together with fluvio-aeolian landforms (e.g. deflation basins and ephemeral lakes).

Fluvial fill terrace

The present day wetland is developed along the part of the fluvial system that has incised into a fluvial terrace (Fig. 2); previously, this terrace incision has been reported only from the northern part, between the "de la Barda" arroyo and the avulsion channel of the Butaló arroyo (Zárate et al. 2005). The analysis carried out for this study enables determination of an extensive areal distribution of the fluvial terrace, which extends across most of the central and southern parts of the study area but is mostly covered by aeolian landforms. Remote sensing analysis was used to identify a distributary channel pattern on the terrace surface, particularly in the northern part (Fig. 2).

The sedimentary composition of the fluvial terrace (i.e. a fill terrace, sensu Bull, 1990) is depicted by three representative sections. At *Arroyo de la Barda 3 section* (located in the northern part of the wetland—Figs. 2, 3 and Table 2), the deposits consist of horizontal and tabular fine-grained layers dominated by silty sand and sandy silt layers, with abundant to moderate content of both gypsum and calcium carbonate, and common Fe-oxide specks (Table 2). Here, a buried soil of weak development (Ab, Cb soil sequence—Table 2: 2.95–3.30 cm depth interval) is discontinuously traceable along the section. Below the buried soil, a discrete limnic level (~ 3.30 m depth, Arroyo de la Barda 3—Fig. 3, Table 2) was dated to 3936 ± 23 ^{14}C yrs BP (4186–4419 cal yrs BP). The alluvial deposits are covered by aeolian silty sands modified by the present soil formation (A, C soil sequence). The ***Chadileuvú I section*** (Figs. 2, 3 and Tables 1, 2), a 5 m thick sedimentary section of the Desaguadero River bank, is composed of muddy and sandy layers (Fig. 3, Table 2) arranged in locally interbedded horizontal tabular layers. The ***Arroyo Gran Barranca section*** (Fig. 2, Table 2), is a ~ 5.5 m thick section made up of alternating tabular layers of massive to locally cross bedded sand to silty very fine sand and sandy silt to muddy layers. Gypsum and calcium carbonate nodules are very common (Fig. 3, Table 2).

The fluvial fill terrace is covered by vegetated aeolian deposits. The remote sensing analysis carried out in this study enables the identification of a wide diversity of dune morphologies. Dunes are generally characterized by a predominant SW–NE oriented linear pattern, previously interpreted as longitudinal dunes (Urbiztondo 1974; Melchor and Llambías 2004; Zárate et al. 2005). In the northern part (~ 36º S) of the study area, there are low relief (~ 1.3 m thick) patches of vegetated dunes with no appreciable morphology and a poorly developed present-day soil (A, C horizons) on top (36º I section in Table 2, Fig. 3). South of ~ 36° S, most of the SW–NE oriented linear pattern consists of parabolic dunes with superimposed NW–SE oriented transverse barchanoid dunes, i.e. complex parabolic dunes (Fig. 4). Parabolic dunes are abundant discrete landforms of low relief (~ 1–3 m) with U-shaped noses, and a length ranging from 1 km up to ~ 5–8 km (mega-parabolic) (Fig. 4a–e). They are in general well-defined landforms, and in some cases are superimposed on palaeochannels on the fill terrace (e.g. in Fig. 4a). Other moderate and more poorly defined parabolic dunes are evidenced by changes in the vegetation

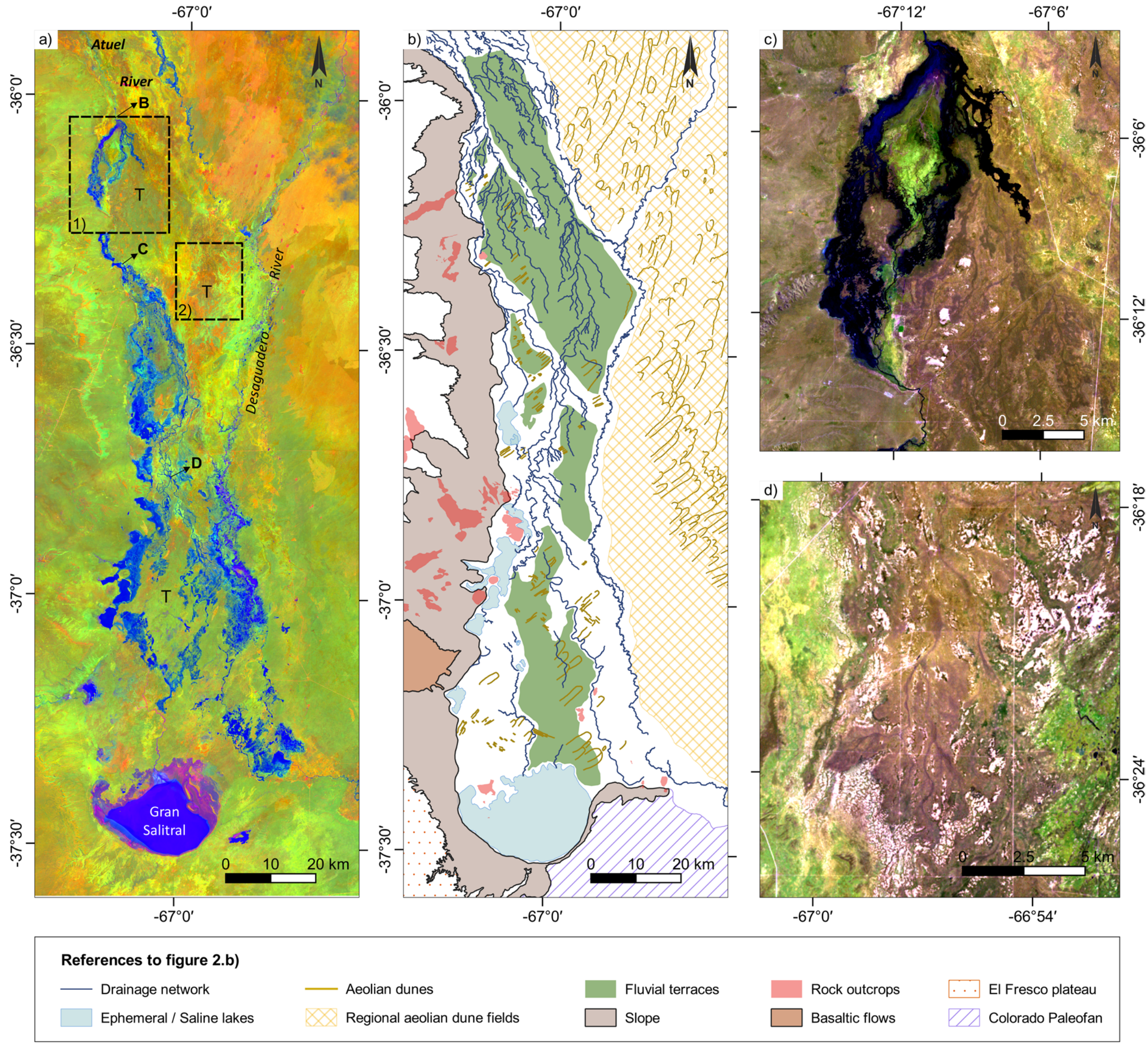

Fig. 2 Bañados del Atuel wetland: **a** two-Landsat-images mosaic (LT05_L1TP_230085_ 19840930_20170220_01_T1 and LT05_L1TP_230086_19840930_ 20170220_01_T1) cut-out with a Tasseled Cap transformation highlighting the fluvial fill terrace (T) unit and the drainage network (blue and light blue colors) in the present-day wetland during the 1984 flood event. Avulsion points B, C and D (described in the text) are indicated; **b** preliminary mapping of the main landscape units identified in the study area; **c**–**d** distributary fluvial pattern on the surface of the fluvial terrace (areas in purple, violet and brown colors in LT05_L1TP_230085_ 19840930_20170220_01_T1; RGB 753) at two locations in the wider study area (Fig. a, boxes 1 and 2)

cover density (Fig. 4c, d, e). Some other dunes present a linear pattern but it is not possible to discriminate if they are longitudinal or parabolic dunes (Fig. 5a, box 1, and b). These dunes are characterized by abundant to moderate gypsum and calcium carbonate content at a depth of ~ 20 cm (Fig. 5c), and the interdunes are characterized by a more abundant but shallower salt content (Fig. 5d). The western part of the study area presents likely diffuse parabolic dunes composed of silty sands and common angular clasts of variable size (Table 2: RP.14 III section, Figs. 3 and 7a, box 2). Finally, in the southern part, there are well defined NW–SE oriented transverse barchanoid dunes (~ 1–2 m high and 100 m wide).

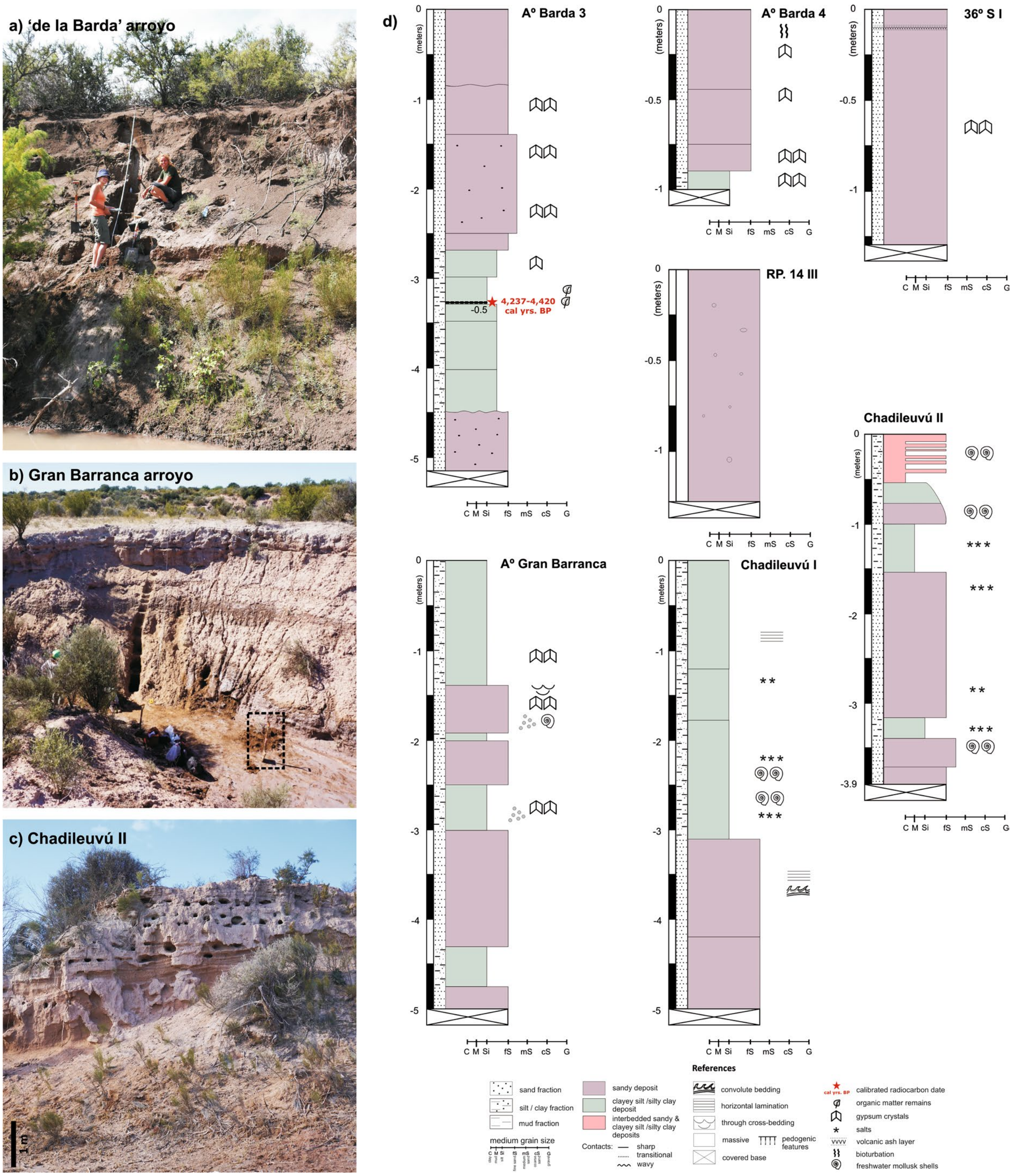

Fig. 3 Fine-grained sedimentary sections representative of the fluvial fill terrace unit (for locations, see Fig. 1b; A° refers to arroyo). **a** ~ 5 m thick terrace section at the 'de la Barda' arroyo, with a calibrated radiocarbon age indicated; **b** ~ 5 m thick sedimentary section at Gran Barranca arroyo, with a shovel for scale; **c** view of the upper section of the fluvial terrace at the Chadileuvú II section; **d** example sedimentary sections from sites associated with the features in parts **a** through **c**

Table 2 Description of sedimentary sections representative of the fluvial fill terrace unit in the Bañados del Atuel wetland

Sedimentary section	Depth range (cm)	Grain size	Geometry—sedimentary structure	Other features	
36º S I 36° 0′2"S, 67° 3′56"W Pit section	0–8	Silty sand	Horizontal and tabular. Massive	Loose. Grayish brown (10 YR 5/2) Common roots Scarce gypsum and $CaCO_3$** (1.2%)	
	8–10	Volcanic ash	Horizontal tabular layer 2–4 cm thick	Light gray (10 YR 7/1)	
	10–35	Silty sand	Horizontal and tabular. Massive	–	Loose. Grayish brown (10 YR 5/2) Scarce gypsum and $CaCO_3$ nodules of variable sizes. 2.1% of $CaCO_3$ in the sedimentary matrix. Low OM* content: 0.29 – 0.31
	35–57			Scarce clay nodules up to 1–2 mm	
	57–130			Scarce clay lenses	
Aº Barda 3 36° 14′27" S, 67° 10′ 55" W Section at the A° de la Barda cut bank	0–295	Silty very fine to medium sand (~83.58% sand, 12.49% silts and 3.93% clay at depth of 40 cm), with sparse granules and clay clast/nodules	Horizontal and tabular Massive	Loose Gray (10YR 5/1), dark gray (10YR 4/1) Fe-oxide mottles in contact with modern roots and restricted to the upper part Abundant gypsum in some levels OM: 0.16 to 0.39%. $CaCO_3$: 0.6 to 5.2%	
	295–330	Silt	Angular to subangular blocky pedological structure	Reddish brown (10 YR 5/4) Contacts: clear and irregular Moderate bioturbation OM value of 0.52%. $CaCO_3$: abundant 3936 ± 23 ^{14}C yrs BP (4186 – 4419 cal yrs. BP; lab code: AA107927) at a depth of ~ 3.30 m	
	330–450	Sandy silt (~ 49.2% sand, 39.87% silts, 10.93% clay) with clay nodules	Horizontal and tabular Laminated (5–8 cm-thick) in the base and massive upward	Grayish brown (10 YR 5/2) passing downward to brown (10 YR 5/3) - reddish brown(10 YR 5/4)	
	450–515	Silty very fine to edium sand	Horizontal and tabular Massive	Loose. Dark grayish brown (10YR 4/2). Clay clasts and nodules. Upper contact: transitional	

Table 2 (continued)

Sedimentary section	Depth range (cm)	Grain size	Geometry—sedimentary structure	Other features
A° Barda 4 36° 15′ 29" S 67° 4′ 59" W Pit section	0–69	Poorly selected silty sand layers	Horizontal and tabular Massive	Light grayish brown (10YR 6/2) to light gray (10YR 7/2) Moderate bioturbation OM: 0.44 to 0.77%. $CaCO_3$: 1.4 to 2.75%, diminish from bottom to top Moderate to scarce gypsum and nodules Scarce Fe-oxide mottles in the lower part
	69–100	Silt		Brown (7.5 YR 5/2). Abundant gypsum nodules. Moderate to abundant $CaCO_3$ Fe-oxide mottles: moderate
RP. 14 III 36° 42′ 39" S 67° 8′ 24" W Pit section	0–130	Silty sand (82.26% fine to medium sand, 13.12% silt, 4.62% clay) with common angular clasts from Late Miocene deposits and rock basement	Horizontal and tabular Massive	Light brownish gray (10 YR 6/2) $CaCO_3$: 1.43% OM: ~0.3%

Table 2 (continued)

Sedimentary section	Depth range (cm)	Grain size	Geometry—sedimentary structure	Other features
Aº Gran Barranca 37° 18′ 4.89" S 66° 58′ 1.26" W Section at the A° Gran Barranca cut bank	0–80	Sand	Horizontal and tabular Massive	Loose Light grayish brown (10YR 6/2)
	80–140	Sandy mud (~ 12.05% sand, 52.74% silts, 35.17% clay)		Moderately firm Moderate to abundant HCl reaction
	140–190	Sand		Loose Light grayish brown (10YR 6/2)
	190–200	Silt with sandy lenses		Moderately firm Moderate to abundant HCl reaction
	200–250	Silty sand (~ 80.76% sand, 15.94% silt, 3.3% clay); sparse granules and gravels	Horizontal. Crossbedded in the upper 10 cm and massive below	Light grayish brown (10YR 6/2) Abundant gypsum, in nodules and forming rhyzoconcretions Freshwater mollusk shells. $CaCO_3$ nodules
	250–300	Silt	Horizontal and tabular Massive	Moderately firm Reddish brown (10 YR 5/4) Gypsum and $CaCO_3$ in the sedimentary matrix (moderate to abundant HCl reaction)
	300–435	Sand (~ 91.55% sand, 24.03% silt, 3.62% clay) with a 4 cm thick silty layer at 330 cm depth		Loose Light grayish brown (10YR 6/2)
	435–475	Mud (~ 9.95% sand, 51.73% silts, 38.31% clay)		Moderately firm Reddish brown (10 YR 5/4) $CaCO_3$ in the sedimentary matrix (moderate to abundant HCl reaction)
	475–495	Sand		Waterlogged
	> 495	Silt		

Table 2 (continued)

Sedimentary section	Depth range (cm)	Grain size	Geometry—sedimentary structure	Other features
Chadileuvú I 37° 21′ 17.04" S 66° 40′ 19.19" W Section at the Desaguadero river cut bank	0–120	Silty clay passing upward transitionally to silt	Laminated in the lower ~ 70 cm, passing transitionally to massive in the upper part	Reddish Brown (10 YR 5/4) Moderate content of nodules gypsum $CaCO_3$: moderate reaction to HCl –
	120–214	Mud (~ 3.26% sand, 50.24% silts and 46.5% clay)	Horizontal and tabular Massive	
	214–309	Sandy silt		Slightly firm. Gley colors Abundante Fe oxides Modern roots. Bioturbations Freshwater mollusk shells Common gypsum nodules $CaCO_3$: poor to moderate reaction to HCl
	309–409	Fine to medium sand in the lower (with a layer of intraclasts) and upper parts; silty sand in the medium part	Horizontal and tabular Massive in lower and upper parts; with convolute bedding in the topmost part. Horizontal and wavy lamination in the medium part	Firm Light grayish brown (10YR 6/2) $CaCO_3$: moderate reaction to HCl
	409–504	Fine to medium sand (~ 95.11% sand, 4.26% silts, 0.63% clay)	Horizontal and tabular Massive	Loose. Light grayish brown (10YR 6/2) Modern roots in the deposit

Table 2 (continued)

Sedimentary section	Depth range (cm)	Grain size	Geometry—sedimentary structure	Other features
Chadileuvú II 37° 21′ 25.56" S 66° 39′ 27.09" W Section at the Desaguadero river cut bank	0–54	Sand, silt	Alternance of sandy and silty massive layers (~ 15–10 cm thick)	Firm in the lower part, moderately firm in the upper part Light grayish brown (10YR 6/2) Abundant modern roots and freshwater mollusk shells
	54–100	Silt passing upwards transitionally to fine-medium sand	Horizontal and tabular Massive	
	100–156	Sandy silt and fine sand	Alternance of sandy silt and fine sand massive layers	Light grayish brown (10YR 6/2) Abundant gypsum nodules
	156–316	Very fine to fine sand in the lower part, alternating with silt layers in the upper part	Massive in the lower part with diffuse bedding upwards (alternance of sandy and silty layers)	Moderately firm Brown (10YR 4/3, sands) and pale brown (10YR 6/3, silts) Abundant gypsum and $CaCO_3$ in the sedimentary matrix, diminishes to the lower part
	316–339	Sandy silt	Horizontal and tabular Massive	Scarce modern roots. Abundant gypsum and $CaCO_3$ in the sedimentary matrix
	339–370	Fine to medium sand with silty clay intraclasts of various sizes		Abundant freshwater mollusk shells
	370–390	Very fine to fine sand		An interbedded level with gley color

*OM: organic matter. **$CaCO_3$: calcium carbonate. * and ** are either numerical percentage or relative concentration, depending on the availability of lab data

They have developed on top of the parabolic dunes on the fluvial terrace and locally form clusters of dunes (up to 1 km long, 300 m wide) towards the E-NE of palaeochannels.

Present-day wetland

The present-day wetland developed after formation of the fill terrace. According to its geomorphological characteristics, three main settings are differentiated: (1) a floodplain environment; (2) a transfer area; and (3) a terminal closed basin (i.e. the Gran Salitral depression, a ~ 450 km^2 salt pan).

(1) The *floodplain* is a NW–SE oriented fluvial channelled environment of ~ 2800 km^2 along both the Atuel River and a reach of the Desaguadero River (Figs. 1a–b, 2a); it is characterized by active and inactive channels, and includes the interdune settings of the SW–NE oriented dune system at some locations (Fig. 5a, box 2). The "de la Barda" arroyo, the westernmost branch of the Atuel River (Figs. 1b, 2), exhibits an anabranching pattern along some reaches, as well as a small number of crevasse channels associated with meanders. Four main avulsion points (Fig. 2a B, C and D) have been identified linked to the "de La Barda" arroyo, and are characterized by distributary systems made up of shallower channels with increasing width/depth ratio as channel divergence progresses downstream (Fig. 2a). At avulsion point A (~ 35° 40′ 36.09″ S, 67° 24′ 28.81″ W), the ~ 60 km long "de los Ingenieros" arroyo was formed, and now feeds the northern portion of the wetland. The 36º S II section, in the floodplain of this arroyo, is composed of horizontal, tabular and massive layers of sandy silts, silts and silty muds that are interbedded with clay layers, resulting in a dominantly horizontal lamination (Fig. 1b, Table 3). Organic matter at a depth of ~ 0.75 cm yielded an age of 914 ± 20 ^{14}C yrs BP (729–895 cal years BP) (Tables 1, 3). Avulsion point B (Fig. 2a) is characterized by a distributary channel pattern, including the Butaló arroyo (~ 4 m deep) that was active during the 1984 flood (Zárate et al. 2005; Dornes et al. 2016). At avulsion point C, downstream of point B and to the north of Algarrobo del Águila locality (Figs. 2a and 5a), the "de la Barda" arroyo splits into three main channels a few kilometres apart from each other (Fig. 5a—ab1, ab2 and ab3); the channels in the SE with numerous splays are currently inactive (Fig. 7a). The floodplain between these channels (Fig. 2—RP. 14 II section) comprises horizontal and tabular, massive, muddy to silty layers. These layers grade upwards into laminated, silty sands with freshwater mollusc shells that yielded an age of 2746 ± 21 ^{14}C years BP (2755–2864 cal years BP) at a depth of ~ 0.40 cm (Fig. 8, Tables 1 and 3). Avulsion point D, located downstream from avulsion point C, resulted from a former avulsion of the "de la Barda" arroyo. An ~ 25 km long, sinuous, SE oriented channel with a distributary pattern is characteristic; shallow and narrow channels linked to discrete depositional lobes are developed along the ~ 12 km long terminal reach (Fig. 7b).

Salt flat depressions are common landforms in the present wetland (Figs. 6, 7a), and are generally situated along high sinuosity channel reaches. The depressions are interconnected during flooding episodes and turn into relatively large ephemeral lakes along the terminal reach of the "de la Barda" arroyo (Fig. 7a), south of Algarrobo del Águila locality. Low relief (~ 2 m) dunes are usually present at the E-NE margin of the depressions (e.g. Fig. 7a, Laguna Uncal in box 1). The location, shape and occurrence of the dunes at the E-NE margins indicate the widening of inactive meanders by winds blowing from the S-SW that lead to deflation. Also, smaller depressions (diameters up to 100 m) of circular shape and low relief (< 1 m height), together with several others of irregular shape (main axis ~ 500 m long), are common throughout the floodplain; clayey silts accumulate in these depressions where hydromorphic soils with halophile vegetation are developed.

In addition, narrow and linear aeolian SW–NE oriented streaks of low relief (< 1 m) occur in the middle sector of the floodplain (~ 36° 42′ 2.64″ S, 67° 4′ 18.39″ W); they are cross cut by an almost perpendicular set of linear, very shallow channels (Fig. 7a, box 2). The result is a reticulate-like pattern formed on the fine-grained and cohesive deposits of the floodplain (Fig. 7b).

(2) The *transfer area* lies in the west-central part of the wetland (Fig. 9a, box 2). It includes two channels, the Potrol and Gran Barranca arroyos, both of which are incised in the fill terrace and connect the NW–SE oriented floodplain with the terminal closed basin (the Gran Salitral—Fig. 9a–c). The Potrol arroyo is linked to the "de la Barda" arroyo by a series of interconnected saline lakes. At present, it is an entrenched channel with active headcut retreat into alternating,

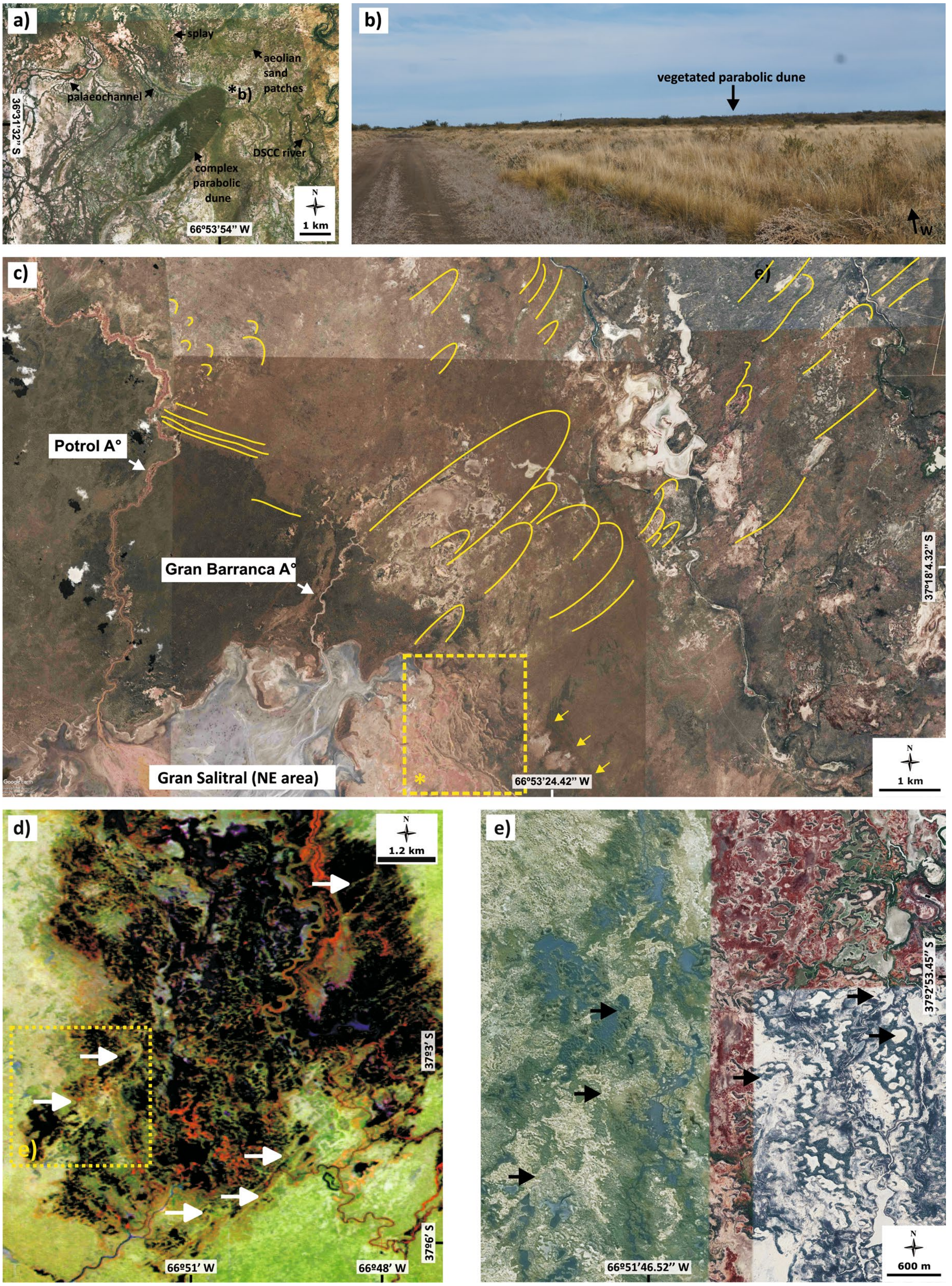
a)
splay
aeolian sand patches
palaeochannel
*b)
DSCC river
complex parabolic dune
36°31'32" S
66°53'54" W
1 km
b)
vegetated parabolic dune
W
c)
e)
Potrol A°
Gran Barranca A°
Gran Salitral (NE area)
*
66°53'24.42" W
37°18'4.32" S
1 km
d)
1.2 km
e)
37°3' S
37°6' S
66°51' W
66°48' W
e)
37°2'53.45" S
66°51'46.52" W
600 m

◂**Fig. 4** Aeolian landforms covering the fluvial fill terrace unit: **a** complex parabolic dune superimposed on a palaeochannel, also with some splays and aeolian sand patches; **b** view to the west of the parabolic dune; **c** low relief parabolic dunes of different sizes and some long NW–SE oriented dunes (yellow lines and arrows) to the north-northeast of the Gran Salitral. A young generation of transverse barchanoid dunes is widely distributed in the area; **d** parabolic dunes (white arrows) close to the Desaguadero River indicated in a Landsat 5 image (year 2006, path 230, row086; RGB453); and **e** enlarged view of box e, indicated in part d. (Parts **a**, **c** and **e** are Google Earth © image captures)

tabular layers of fine sand and silty fine sand that contain freshwater mollusc shells of a desiccated shallow lake; the channel is progressively deeper (6–7 m) and somewhat wider (up to ~ 50 m) downstream (Figs. 9a–b). The Gran Barranca arroyo (5–6 m deep) (Fig. 9a and c) is much shorter, and also characterized by active headcut retreat. This process is also developed along the lower reaches of the minor tributaries and gullies. Upstream, the Gran Barranca arroyo is connected by a chain of small shallow lakes and pans with a channel resulting from the junction of two fluvial branches, one moderately to poorly defined coming from the "de La Barda" arroyo and the other, very distinct and well defined, from the Desaguadero River (Fig. 9a, box 2).

(3) The Gran Salitral is a *terminal closed basin* at the tip of the system; an endorheic depression of ~ 450 km^2 (main axis of 22 km N-S × 28 km E-W) with a relative relief of 7 m (lowest point 247 m asl, 254 m asl at the shoreline). A tectonic origin was attributed to the depression, supposedly controlled by NE and NW oriented fault lines on the basis of the rectilinear aspect of the shorelines (Bisceglia 1997 in Melchor and Casadío 2000, p. 49). The Gran Salitral is bounded by the Colorado palaeofan to the south and El Fresco plateau to the west (Figs. 1a, 9a, 9d and 9e). The depression is a temporary water storage during major hydrological episodes; to date, it is only reached by exceptional seasonal discharges of the fluvial system (e.g. years 1984 and 2007) when it turns into an ephemeral shallow saline lake. When dried out, deflation is active. Sandy deposits and evaporites including organic remains have been reported in the uppermost metre of the sedimentary fill (Melchor and Casadío 2000). NW–SE oriented transverse barchanoid dunes are present in the central part as well as in the N-NE sector (Fig. 4c, box); also, NW–SE oriented dunes (~ 6 km long, 1–2 m relative relief) occur ~ 2 to 3 km away from the present shoreline and are masked by a dense vegetation cover (Fig. 4c).

Holocene evolution of the wetland

The fluvio-aeolian plain of the Bañados del Atuel is dominated by Holocene fine-grained deposits composed of massive and/or laminated tabular layers mostly related to overbank flooding and/or sheet flooding in a floodplain setting. Organic matter content is limited and calcium carbonate and gypsum content is moderate to abundant. These sedimentological features point to a predominantly dry environment comparable to those reported from other arid zone wetlands (Tooth and McCarthy 2007).

According to the radiocarbon dates obtained, the fluvial fill terrace developed after an erosional episode sometime in the mid-late Holocene transition, i.e. after 4186–4419 cal years BP (age obtained in the fill terrace deposits) but before 2755–2849 cal years BP (age of floodplain deposits in the present-day wetland environment). The fill terrace distribution suggests a much larger extension of floodplain environments of the Atuel River in the study area prior to the late Holocene. The fluvial terrace records a distributary fluvial pattern (identified by remote sensing analysis) in the northern part of the study area. On the other hand, the arrangement of alternating, tabular, fine-grained deposits at the Gran Barranca arroyo is a record of sheet flood deposition and points to a terminal sedimentary setting similar to a floodout zone (Tooth and Nanson 2011).

The fill terrace along the Bañados del Atuel is correlated with a comparable landform along the Atuel River ~ 200 km upstream. There, an extensive geomorphological unit is exposed, with a ~ 12 m thick alluvial section composed of alternating, tabular and horizontal, massive layers of sandy silts, silty sands and mud (Zárate and Mehl 2011). Reported radiocarbon dates indicates an early (10,180–10,300 cal years BP) to mid Holocene (7156–7425 cal years BP) age for the bottom and middle parts of the fill terrace; an erosional episode then occurred later in the mid Holocene (Zárate and Mehl 2011).

The fluvial systems in the proximal Andean piedmont of Mendoza, to the north of the Atuel River basin, record two major episodes of incision in the mid and late Holocene. At La Estacada arroyo (33º

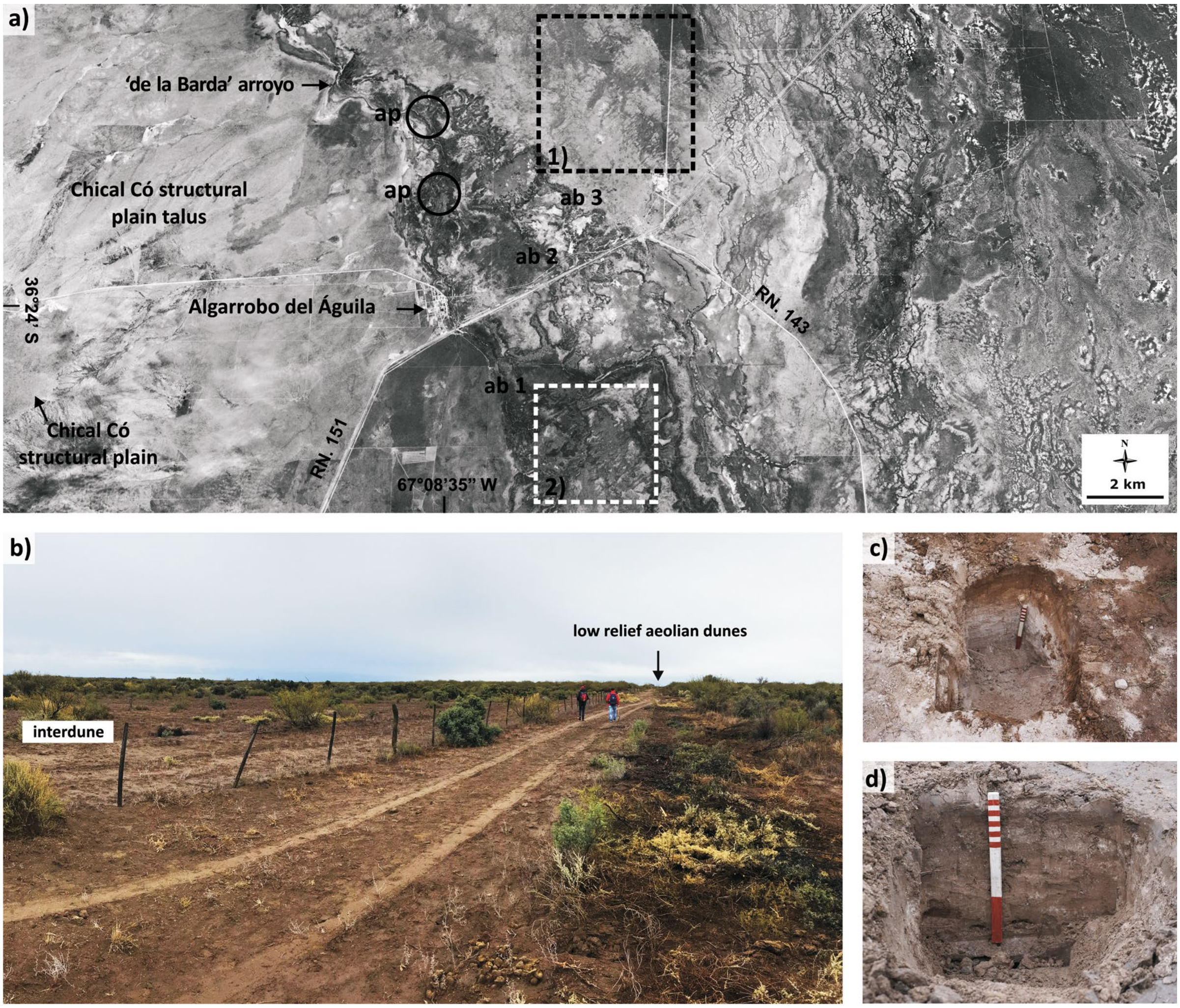

Fig. 5 Fluvial terrace and floodplain in the present-day wetland: **a** avulsion point B along a reach of the 'de La Barda' arroyo and channels developed downstream (ab1-3). SW–NE oriented aeolian linear streaks are evident on the fluvial terrace (box 1) and on the present-day floodplain wetland (box 2). National routes RN 143 and 151 are shown; **b** view in the field of low relief, fine sandy aeolian linear streaks that cover the fluvial terrace deposits; **c** excavation pit in the aeolian deposits, showing abundant salts (calcium carbonate and gypsum) concentrated below 20 cm depth; **d** excavation pit in the interdune area, showing silty and clayey sediments and salts efflorescences

26′ 52″ S, 69º 03′ 09″ W), the first episode of fluvial incision occurred sometime during the mid Holocene and was followed by aggradation. At the Yaucha arroyo (34º 03′ 54″ S, 69º 08′ 06″ W), two episodes of channel incision are also recorded. The first one occurred sometime between 6500 cal years BP and well before 2622–2857 cal years BP, and was followed by fluvial aggradation. The hypothesis is that climatic fluctuations occurring prior to at least 5700 cal BP may have triggered the first episode of fluvial incision in this piedmont location (Mehl and Zárate 2012). More humid conditions in the high Andes, due to a northern shift of the westerlies and likely greater fluvial discharges in the Andean rivers, coupled with much drier conditions across the eastern piedmont, may have characterized the climatic scenario (Mehl and Zárate 2012 and references therein).

The timing of the mid to late Holocene episode of incision in the study area is not precisely constrained.

Table 3 Description of sedimentary sections representative of the present-day floodplain wetland environment

Sedimentary section	Depth range (cm)	Grain size	Geometry—sedimentary structure	Other Features	
36º S II 36° 0′ 2" S, 67° 4′52" W Pit section Floodplain with bare soil	0–15	Silt	Horizontal and tabular Massive	Moderately bioturbated, Fe oxide mottles and roots	Brown (10 YR 5/3)
	15–32	Sandy silt		Moderate $CaCO_3$** and gypsum around roots	
	32–52	Silt and clay	Horizontal and tabular Lamination (interbedded silt and clay laminae), passing upwards to a wavy lamination	Firm. Greyish brown (10 YR 5/2) Moderate $CaCO_3$ and bioturbation	
	52–74	Mud		Pale brown (10 YR 6/3). Moderate $CaCO_3$, gypsum and Fe oxide mottles	
	74–85	Silt	Horizontal and tabular Massive Weak pedological structure	Very dark gray (10 YR 3/1) and gray (10 YR 5/1) Scarce $CaCO_3$ in the base. Abundant bioturbation. Low OM* content (0.6%) 914 ± 20 ^{14}C yrs BP (729 – 895 cal yrs. BP; lab code: AA107929) at a depth of ~ 74 cm	
	85–100	Mud	Horizontal and tabular Massive	Firm. Grayish brown (10 YR 5/2) Abundant $CaCO_3$ (0.9-a 8.8%) Moderate bioturbation OM: 0.52 – 0.94%	
36º S III 35° 59′ 58" S, 67° 6′ 34" W Pit section. Floodplain with desiccation cracks on surface	0–45	Mud	Horizontal and tabular Massive	OM: 0.58% $CaCO_3$: 4.16% Common plant fragments and roots	
A° Barda 1 35° 59′ 58" S, 67° 11′ 6" W Pit section Thalweg of an inactive channel	0–160	Medium to coarse sand with with abundant granules and very fine-fine pebbles	Horizontal and tabular Trough cross-bedded; interbedded 3 cm-thick sandy lenses	Greyish brown (10 YR 5/2) Freshwater mollusk shells OM: 0.11%. $CaCO_3$: 2.4%	
	160–220	Sand with interbedded sandy silt layers	Horizontal and tabular Massive to laminated	Brown (10 YR 5/3) OM: 0.17%. $CaCO_3$: 4%	
	220–250	Sandy silts		Greyish brown (10 YR 5/2) OM: 0.47%. $CaCO_3$: 6.6%	

Table 3 (continued)

Sedimentary section	Depth range (cm)	Grain size	Geometry—sedimentary structure	Other Features	
A° Barda 2 36° 3′ 1" S, 67° 10′ 50" W Section at the A° de la Barda cut bank	0–83	Sandy silts with interbedded sand layers and 2 mm-2 cm thick sandy clay layers	Horizontal and tabular Interbeded layers with laminated aspect, occasionally wavy lamination	Grayish brown (10 YR 5/2), downward gray (10 YR 5/1) Slightly bioturbated Scarce Fe-oxide mottles	OM: 0.3–0.01% CaCO3: 4.8–1.8%, diminish from bottom to top
	83–200	Medium to coarse sand with a lense (10-cm-thick) of silt and with clay granules	Horizontal and tabular Trough cross-bedded	Dark gray (10YR 4/1) Fresh mollusk shells	
RP. 14 I 36° 42′ 33" S, 67° 2′ 15" W Pit section Thalweg of a currently inactive channel	0–19	Sandy silts in the upper 5 cm, below silts	Horizontal and tabular Horizontally laminated with some convolute bedding features and massive structure in the upper 5 cm	Very dark gray (10 YR 3/1) Common roots in the upper 5 cm with	
	19–35	Silt	Angular to subangular blocky structure	Very dark gray (10 YR 3/1) Slight to moderate bioturbation and Fe-oxide mottles. Common cutans Lower part: abundant bioturbation and scarce freshwater mollusk shells	
	35–54	Sandy silts	Horizontal and tabular Massive	Very dark gray (10 YR 3/1) Scarce $CaCO_3$ and gypsum Lower part: abundant bioturbation	
	54–66			Light gray (10 YR 7/1). Scarce Fe oxide mottles Upper part: abundantbioturbation	
	66–120			Light gray (10 YR 7/1). Common Fe oxide mottles. Moderately bioturbated OM: up to 4.6% in the upper part $CaCO_3$: 3–0.6%, diminishing downward	

Table 3 (continued)

Sedimentary section	Depth range (cm)	Grain size	Geometry—sedimentary structure	Other Features
RP. 14 II 36° 42′ 36" S, 67° 4′ 57" W Floodplain	0–20	Sandy silt	Horizontal and tabular Massive	Slightly firm Abundant roots in the upper 4 cm and gray (10 YR 5/1); below: gray (10 YR 6/1), with abundant gypsum and abundant to moderate $CaCO_3$
	20–43			Slightly firm. Light gray (10 YR 7/1) Abundant gypsum. Abundant bioturbation Common freshwater mollusk shells
	43–64			Slightly firm. White (10 YR 8/1) Abundant bioturbation. Moderate Fe oxide mottles. Common freshwater mollusk shells $CaCO_3$: 28.8%. 2746 ± 21 ^{14}C yrs BP (2755 – 28,645 cal yrs. BP; lab code: AA109605) at a depth of ~ 45 cm
	64–81	Silt		Firm. White (10 YR 8/1) with gley color mottles. Abundant bioturbation Abundant gypsum
	81–115	Mud		Slightly firm. Pinkish gray (7.5 YR 6/2) Abundant bioturbation. Upper and bottom parts: scarce $CaCO_3$, abundant gypsum in the sedimentary matrix and 0.47 to 0.93% OM Moderate Fe oxide speckles Common freshwater mollusk shells Medium part: 28% $CaCO_3$

*OM: organic matter. **$CaCO_3$: calcium carbonate. * and ** are either numerical percentage or relative concentration, depending on the availability of lab data

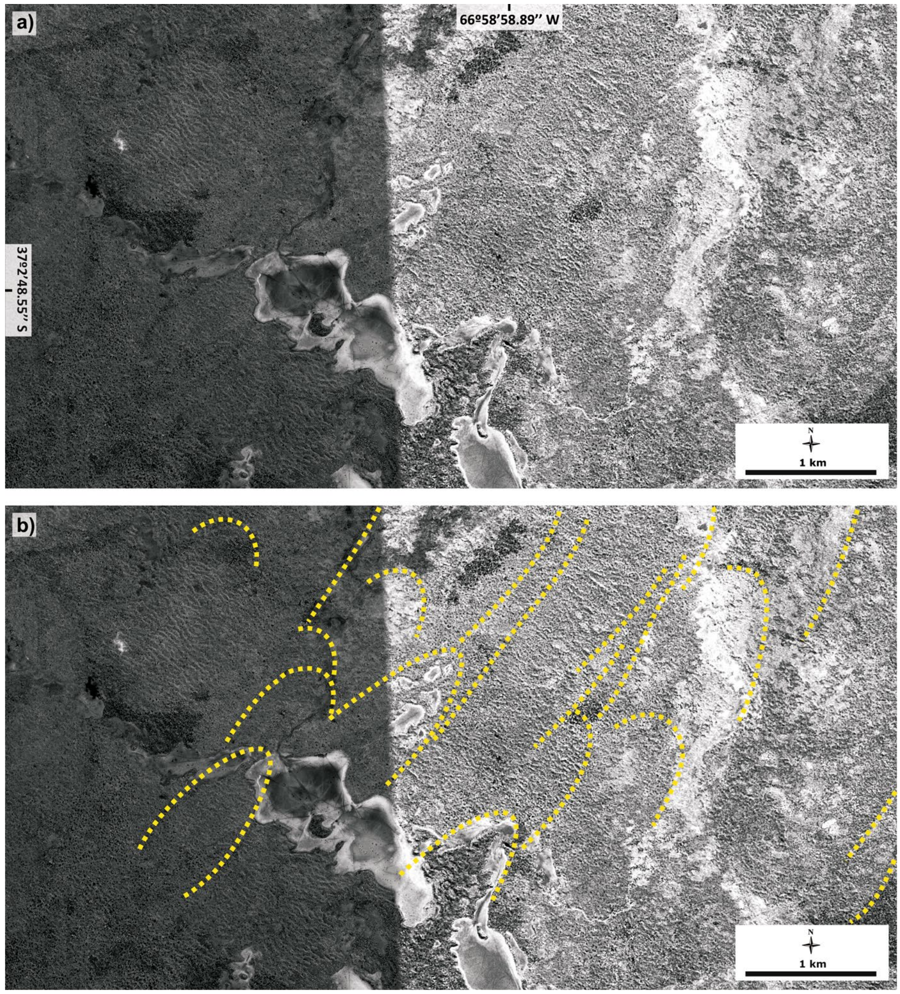

Fig. 6 Aeolian cover on the fluvial fill terrace unit: **a** parabolic dunes and/or SW–NE linear streaks and transversal barchanoid dunes (Google Earth © image capture); **b** annotated image, highlighting the main aeolian features

However, according to the chronostratigraphic regional framework, we can speculate that the establishment of similar-to-present climatic conditions in the region (Markgraf 1983) resulted in a major environmental change and could have been a factor triggering incision. In southern South America, the westerlies strengthened during the mid Holocene and their northern boundary shifted farther north because of increased sea-surface temperatures in the eastern subtropical Pacific that were caused by higher austral summer insolation (Lamy et al. 2010). A recent palaeorainfall record based on oxygen isotopes in speleothems from the Mato Grosso do Sul, Brazil, indicates less wet conditions in the South American Monsoon (SAM) domain in the early and mid Holocene (11,000–5550 years BP) compared with the previous last glacial period (27,970–17,800 years BP) (Novello et al. 2017). The authors point to a tendency for a drier Holocene, consistent with other palaeorainfall records from the western and southeastern portions of the SAM domain. Coupled simulations indicate a less frequent control of El Niño Southern Oscillation (ENSO)—an atmospheric phenomenon that causes significant impacts on seasonal and monthly precipitation amounts in several regions of South America (Grimm and Tedeschi 2015) and is the main mode of sea surface temperature variability in the Pacific Ocean—on precipitation during the mid Holocene over South America (Jorgetti et al. 2006). Karamperidou et al.'s (2015) simulations proposed that the frequency of occurrence of eastern Pacific ENSO events significantly decreased (by 50%) in the mid Holocene. Instead, the late Holocene is characterized by the intensification of the SAM over southeastern

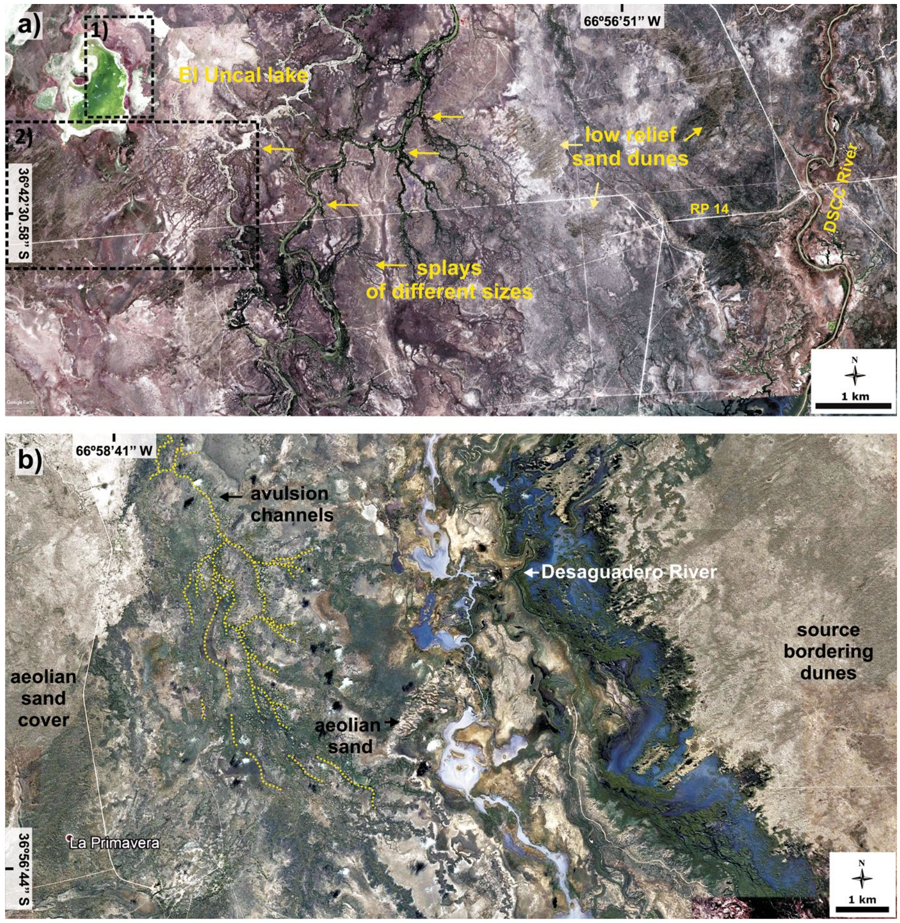

Fig. 7 Remote sensing views of the present-day wetland (Google Earth © image captures): **a** image showing splays of different sizes, isolated patches of low relief dunes covering the alluvial plain, low relief (~2 m) dunes in the E-NE margin of the Laguna Uncal (box 1), and a pattern of fluvio-aeolian interactions (box 2). RP 14 is Provincial Route No. 14; **b** terminal reach of an avulsion channel, showing a distributary pattern in the southernmost wetland area

South America and the increased variability of ENSO (Razik et al. 2013).

The drainage network of the Bañados del Atuel, and the associated lobate shape of many fluvial landforms in plan view, suggest avulsion as the leading fluvial process during wetland evolution. Seismic activity has been proposed as a triggering mechanism to explain the generation of some avulsion points in the wetland (Melchor and Llambías 2004). Avulsion episodes must have occurred under flooding conditions and/or close to the hydrological capacity of this fluvial system that is characterized by a seasonal regime. In this sense, high discharges in the Andean rivers have been linked to ENSO events (historical chronicles in Aceituno et al. 2009; Araneo and Compagnucci 2008). Furthermore, major historical floods in the wetland would also have been connected to those events, e.g. years 1877–1878 (1890s Land Surveys Notebooks La Pampa province Cadastre office) and 1983–1984. Hence, it is plausible to hypothesize that major floods related to ENSO events may have triggered avulsion episodes during the late Holocene. In relation to ENSO events, the study by Wells (1990, in Ortlieb and Macharé, 1993) in the valley of Río Casma, located along the arid north-central Peruvian coast, reported 18 Holocene flood events and a few late Pleistocene flood remnants. Wells (1990) highlighted a mean frequency of major El Niño events in the order of one episode every 1000 years during the last 7000 years, although many more flooding events were registered in the last few thousand years.

The channel incision of the Potrol and Gran Barranca arroyos is an ongoing process, as indicated by the active headcut retreat. Incision started in the late Holocene and was likely accelerated by the anthropogenic changes during the last 200 years in the fluvial system; i.e. the diverting in 1809 of the Diamante River, a former tributary of the Atuel River (Difrieri

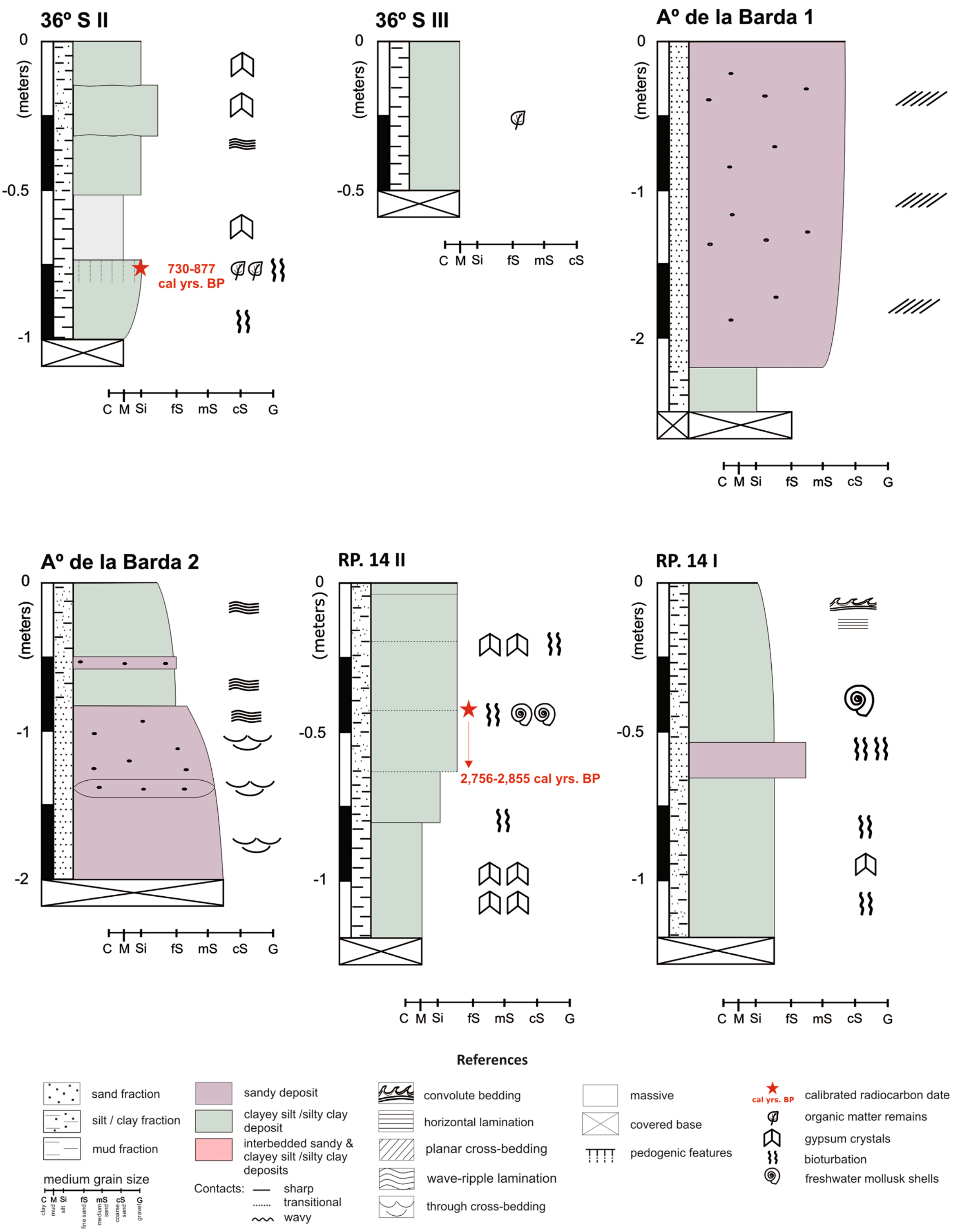

Fig. 8 Fine grained sedimentary sections representative of the present-day floodplain wetland (for locations, see Fig. 1b, and for descriptions, see Table 2)

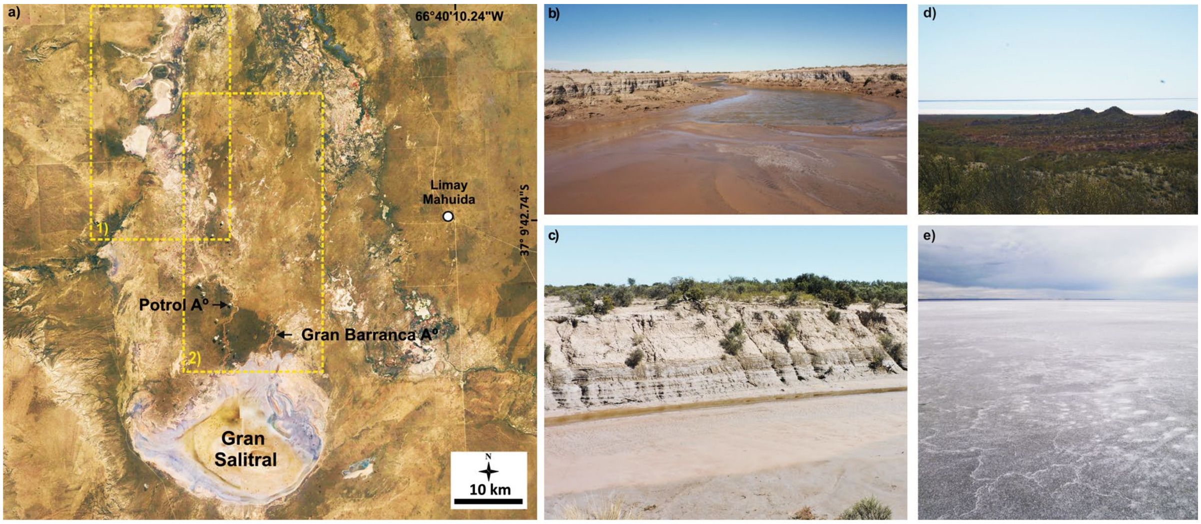

Fig. 9 Middle-south area of the Bañados del Atuel wetland: **a** salt flat depressions in the present floodplain wetland (box 1) and transfer area with headcutting channels entrenched in the fluvial terrace deposits (box 2); **b** and **c** fine-grained and laminated sedimentary deposits exposed along the banks of the Potrol and Gran Barranca arroyos, respectively; **d** view to the north of the Gran Salitral; **e** the Gran Salitral during a desiccation stage; salt crust and desiccation cracks have developed on the surface. Photo courtesy of Lic. Mónica Pires

1980), and the construction of several dams for hydroelectric and irrigation purposes in the mid-twentieth century (Fig. 1a). No new information was obtained to calibrate the evolution of the terminal zone of the wetland, the Gran Salitral. Considering the evidence for a more extensive mid Holocene floodplain, the Gran Salitral most likely was a more permanent water body, as the main allochthonous rivers in the region were active even when there was a regional condition of aridity in Andean piedmont (Gil et al. 2005). The Gran Salitral must have experienced progressive desiccation since the late Holocene onwards, leading to increasing deflation in the basin.

Aeolian processes have generated both erosional (deflation basins) and depositional landforms in the wetland. The latter consists of an aeolian dune field mostly dominated by dune complexes (parabolic dunes with superimposed transverse-barchanoid dunes), inactive under current conditions because of a well-developed vegetation cover and/or a lack of sediment supply resulting from a diminished Atuel River system. The geomorphological relationships of the fluvial and aeolian landforms identified illustrate the interactions of fluvial and aeolian processes (Fig. 10a–d). These interactions seem to have been pronounced at some intervals during the evolution of the present wetland environment.

Two main episodes of dominant aeolian activity are inferred during the late Holocene. The first one was related to parabolic dune formation. Parabolic dunes tend to occur in areas with high groundwater levels and are favoured by the presence of vegetation or dampness in the lower sides of the dunes (Goudie 2011). Vegetation anchors the less mobile parabolic dune arms against aeolian processes and promotes the downwind advance of the central section. Parabolic dunes may replace more active forms such as barchans if vegetation cover increases or wind velocities slacken (Goudie 2011). The second episode of aeolian activity is recorded by the presence of NW–SE oriented transverse barchanoid dunes superimposed on the parabolic dunes. In this regard, Goudie (2011) and Barchyn and Huegnholtz (2012a, b) have stated that parabolic dunes can turn into active transverse dunes if vegetation cover diminishes. Barchan–parabolic transformation occurs via feedback initiated from colonization of vegetation on the dune slipface, which causes the stabilization of individual 'dune slices' (Barchyn and Huegnholtz 2012a, b). This process can only occur when slipface deposition rates are less than the deposition tolerance of vegetation.

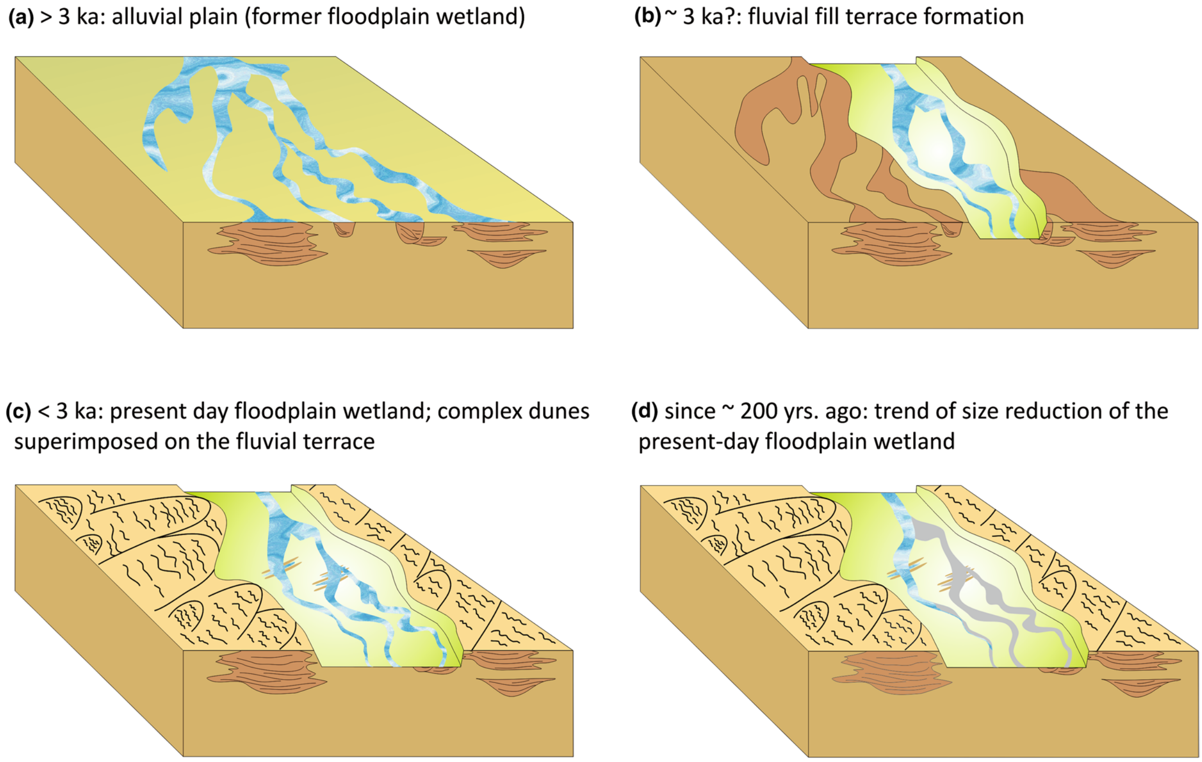

Fig. 10 Schematic diagram depicting four stages of the Holocene evolution of the Bañados del Atuel wetland: **a** an alluvial plain developed before ~ 3 ka; **b** fluvial fill terrace formation owing to incision ~ 3 ka led to decoupling of the former alluvial plain from active fluvial processes along the incised channel; **c** present-day floodplain wetland developed over the last 2–3 millennia. Dune complexes (parabolic dunes with superimposed transverse-barchanoid dunes) cover the fill terrace surface that bounds the present-day wetland. Low relief aeolian dunes also control flow in some reaches of the present-day wetland; **d** the present-day floodplain wetland is subject to a trend of size reduction, starting ~ 200 years ago

In this sense, the formation of transverse dunes in the study area could have been promoted by an arid condition at the late Holocene. The morphology of the dunes (i.e. parabolic dunes with superimposed transverse barchanoid dunes) evidences a likely decrease in the vegetation cover because of more arid conditions.

This pattern of fluvio–aeolian interactions not only resulted in dune complexes covering the fill terrace surface, but also in the dominant SW–NE orientation of the dune systems that controlled the development of the floodplain in the present-day wetland in several sectors. This is suggested by interdune settings of parabolic dunes and the SW–NE oriented aeolian linear pattern that currently is flooded when the wetland is active. Besides, deflation basins are associated with some channel reaches, as indicated by the dunes in the N-NE margin of the depressions.

Regarding these fluvio-aeolian interactions in the study area, some similarities can be found in other drylands; for example, with the Murray-Darling Basin, Australia. There, the main area of dunes—the mallee dunefield—is suggested to have developed as a function of: (1) the spatial environmental transition in the catchment; and (2) the role of the coupled fluvial–aeolian–lacustrine systems in the formation of local source-bordering dunes (Bullard and McTainsh 2003). The formation of channel source-bordering dunes in that region of Australia took place from 5500 years BP to 600 years BP, because of significant sand supply by streams and very hot, dry and windy summer conditions that promoted sand deflation from the channels (Williams et al. 1991, in Bullard and McTainsh 2003). Earlier in the late Holocene, climatic conditions and lower wind speeds precluded the formation of source-bordering dunes; moreover, under current conditions, the dunes are not active because of a well-developed vegetation cover and the lack of sediment supply (Williams et al. 1991, in Bullard and McTainsh 2003). Thus, at present, the fluvio-aeolian system is described as decoupled: aeolian activity is largely separated from the fluvial system (Bullard and McTainsh 2003).

The Bañados del Atuel is located to the southwest and south of a major aeolian system, with large dune fields to the NE and N and extensive aeolian sand mantles to the E. The SW–NE orientation of the parabolic and linear aeolian landforms in the Bañados del Atuel indicates a NE wind transport direction, also recorded in the aeolian environment east of the Desaguadero River (Fig. 2b) (Tripaldi and Zárate 2017). No dates are available to calibrate the chronology of two main intervals with active aeolian activity at the Bañados del Atuel, but according to regional correlations the aeolian activity most likely responded to regional climatic conditions. In central-west Argentina, the reported chronology of dune fields spans the late Pleistocene (Marine Isotopic Stages (MIS) 3 to 2) and the Holocene (MIS 1). A limited number of optically stimulated luminescence (OSL) dates from dune deposits in the central Andean piedmont indicate aeolian activity during the late Holocene. In this regard, ~ 250 km north of the wetland study area, an OSL date of 1610 ± 0.21 yrs BP was obtained from dunes located in the Atuel River basin (Tripaldi et al. 2011). Also, episodes of aeolian accumulation are reported in the Andean piedmont of San Juan province, 500 km north of the study area. Ages of 4000, ~ 2100 600 and 400 yrs BP were obtained at the Médanos Grandes dune field and ~ 2500, 900 and 500 yrs BP at the Médanos Negros dune field (Tripaldi and Forman 2007).

Conclusion

The geomorphological and sedimentological analysis carried out suggests a sensitive Holocene dryland environment characterized by active fluvio-aeolian interactions. The preliminary chronological scheme proposed points to a relatively recent development of the present-day wetland, not older than the late Holocene (i.e. the last 2–3 millennia). The drainage network is mostly characterized by the occurrence of avulsion and the channels have had clear interactions with the aeolian dune systems at several sectors of the wetland (e.g. as evidenced by reticulate patterns, interdune settings controlling water flow in some distributary channels, dunes eroded by fluvial channels, and dunes superimposed on palaeochannels). The ongoing interactions during the evolution of the wetland suggests alternating environmental conditions with periods when fluvial activity decreased and aeolian processes dominated (e.g. formation of dune systems and deflation basins).

The occurrence of a fill terrace covered by dune complexes and with deflation basins, dominant in the west-central part of the study area, provides evidence for much more extensive floodplain environments prior to the early-mid Holocene. According to the correlations through the fluvial basin, the fill terrace represents an aggradation cycle starting prior to the early Holocene, and is then interrupted by an erosional episode later in the mid Holocene. The pronounced decrease of the wetland area and the predominance of aeolian activity at some intervals during the late Holocene suggest prevailing arid conditions with a substantial decrease in water discharges. Superimposed on this late Holocene trend of wetland reduction, the anthropogenic modifications introduced since ~ 200 years ago in the fluvial system have given rise to even more severe changes. As a result, the present wetland has turned into more of a desert setting with deteriorated system functionality and threatened resilience. In this respect, the active headcut retreat in several channels and the present aeolian deflation at numerous pans must have been accelerated by the human impacts on the fluvial system.

Acknowledgements Dr. Florencia Lorenzo's studies were part of a PhD thesis research carried out with a grant of the National Research Council of Argentina (CONICET). We gratefully acknowledge Dr. Adriana Blasi (FCEyN - UNLP) for an early reading of the manuscript. Our gratitude is extended to the two anonymous reviewers, the Editor-in-Chief and the Guest Editor (Professor Stephen Tooth) for their suggestions and comments that improved and strengthened the manuscript.

Author contributions All authors contributed to the conceptualization of the study and its design, field work and the formal analysis and interpretation of data. AEM: funding acquisition; investigation; first manuscript draft; visualization; manuscript writing, reviewing and editing. MAZ: funding acquisition; investigation; supervision; manuscript writing; review. FRL: investigation; GIS software management; review.

Funding This work was funded by PICT 2012-1512 and PICT 2018-02465 from the ANPCyT, and PIO-12CO from CONICET-UNLPam.

Data availability The datasets used and/or analysed during the current study are available from the corresponding author on reasonable request.

Code availability Not applicable.

Declarations

Conflict of interest The authors have no conflicts of interest to declare that are relevant to the content of this manuscript.

Ethical approval Not applicable.

Consent to participate Not applicable.

Consent for publication Not applicable.

References

Aceituno P, Prieto MR, Solari ME, Martinez A, Poveda G, Falvey M (2009) The 1877–1878 El Niño episode: associated impacts in South America. Clim Change 92:389–416. https://doi.org/10.1007/s10584-008-9470-5

Araneo DC, Compagnucci RH (2008) Atmospheric circulation features associated to Argentinean Andean rivers discharge variability. Geophys Res Lett 35:L01805. https://doi.org/10.1029/2007GL032427

Araneo D, Villalba R (2015) Variability in the annual cycle of the Rio Atuel streamflows and its relationship with tropospheric circulation. Int J Climatol. https://doi.org/10.1002/joc.4185

Barchyn TE, Hugenholtz CH (2012a) Predicting vegetation-stabilized dune field morphology. Geophys Res Lett 39:L17403. https://doi.org/10.1029/2012GL052905

Barchyn TE, Hugenholtz CH (2012b) A process-based hypothesis for the barchan–parabolic transformation and implications for dune activity modelling. Earth Surf Proc Land. https://doi.org/10.1002/esp.3307

Benzaquén L, Blanco DE, Bo R, Kandus P, Lingua G, Minotti P, Quintana R (eds) (2017) Regiones de Humedales de la Argentina. Ministerio de Ambiente y Desarrollo Sustentable, Fundación Humedales / Wetlands International, Universidad Nacional de San Martín y Universidad de Buenos Aires, p 333. ISBN: 978-987-29811-6-7

Bull WB (1990) Stream-terrace genesis: implications for soil development. Geomorphology 3:351–367

Bullard JE, McTainsh GH (2003) Aeolian–fluvial interactions in dryland environments: examples, concepts and Australia case study. Prog Phys Geogr 27(4):471–501

Cano E (2004) Inventario Integrado de los Recursos Naturales de la provincia de La Pampa, 2° edición. Instituto Nacional de Tecnológica Agropecuaria – Universidad Nacional de La Pampa (Coord., 493 pp)

Cazenave HW (1979) Sobre algunos fluviogeónimos del área de los ríos Atuel - Salado - Chadileuvú. Administración Provincial del Agua. Gobierno de La Pampa. Unpublished report RA/0037

Criado Roqué P, Ibañez G (1979) Provincia geológica sanrafaelino-Pampeana. In: Turner JCM (ed) Segundo Simposio de Geología Regional Argentina. Academia Nacional de Ciencias, Córdoba, pp 837–869

Difrieri HA (1980) Historia del Río Atuel. Facultad de Filosofía y Letras, Universidad de Buenos Aires

Dornes PF, Buss RG, Secco ND (2013) Influencia de la intermitencia de los escurrimientos en la Cuenca inferior del río Atuel sobre la interacción agua superficial y subterránea. XXIV Congreso Nacional del Agua. San Juan. Argentina. Anales Congreso, 271. ISSN 1853-7685

Dornes PF, Antonena SV, Minig A, Comas RN, Schulz CJ, Mariño EE (2016) Relación entre regímenes de escurrimiento superficiales y subterraneos en los humedales de los ríos Atuel y Salado, La Pampa. In: Rel. Agua Subt.-Sup. García R, Rocha V, Dornes P (Eds), pp. 221–228. IX Cong. Arg. Hidrogeología - VII Sem. Hisp. Latinoamer. Hidrol. Subt. Catamarca. Arg. ISBN: 978-987-661-225-8

Folk RL, Andrews PB, Lewis DW (1970) Detrital sedimentary rock classification and nomenclature for use in New Zealand. N Z J Geol Geophys 13:937–968

Gil A, Zárate M, Neme G (2005) Mid-Holocene paleoenvironments and the archaeological record of Southern Mendoza, Argentina. Quat Int 132:81–94

Goudie A (2011) Parabolic Dunes: distribution, form, morphology and change. Ann Arid Zone 50(3–4):1–7

Grimm AM, Tedeschi RG (2009) ENSO and Extreme Rainfall Events in South America. J Clim 22:1589–1609. https://doi.org/10.1175/2008JCLI2429.1

Heiri O, Lotter AF, Lemcke G (2001) Loss on ignition as a method for estimating organic and carbonate content in sediments: reproducibility and comparability of results. J Paleolimnol 25:101–110

Hogg A, Heaton T, Hua Q, Palmer J, Turney C, Southon J et al (2020) SHCal20 southern hemisphere calibration, 0–55,000 years cal BP. Radiocarbon 62(4):759–778. https://doi.org/10.1017/RDC.2020.59

Jorgetti T, Silva Dias PL, Braconnot P (2006) Review of: El Niño influence over South America during the mid-Holocene. Adv Geosci 6:279–282

Junk WJ, An S, Finlayson CM, Gopal B, Kvet J, Mitchell SA, Mitsch WJ, Robarts RD (2013) Current state of knowledge regarding the world's wetlands and their future under global climate change: a synthesis. Aquat Sci 75(1):151–167. https://doi.org/10.1007/s00027-012-0278-z

Karamperidou C, Di Nezio PN, Timmermann A, Jin F-F, Cobb KM (2015) The response of ENSO flavors to mid-Holocene climate: implications for proxy interpretation. Paleoceanography 30:527–547. https://doi.org/10.1002/2014PA002742

Lamy F, Kilian R, Arz HW, Francois J-P, Kaiser J, Prange P, Steinke T (2010) Holocene changes in the position and intensity of the southern westerly. Nat Geosci. https://doi.org/10.1038/NGEO959

Lorenzo FR (2019) Evolución Geológica de la cuenca inferior del río Atuel durante el Holoceno provincia de Mendoza y La Pampa). PhD thesis. Universidad Nacional de San Luis, San Luis, Argentina

Malvárez AI (1999) Tópicos sobre humedales subtropicales y templados de Sudamérica. Oficina Regional de Ciencia y Técnica para América Latina y el Caribe. Programa Hombre y Biosfera-Organización de las Naciones Unidas para la Educación, la Ciencia y la Cultura, pp. 228. ISBN 92-9089-064-9

Markgraf V (1983) Late and postglacial vegetational and paleoclimatic changes in subantarctic, temperate and arid environments in Argentina. Palynology 7:43–70. https://doi.org/10.1080/01916122.1983.9989252

Mehl AE, Zárate MA (2012) Late Quaternary alluvial records and environmental conditions in the eastern Andean piedmont of Mendoza (33º–34º S) Argentina. J S Am Earth Sci 37:41–59. https://doi.org/10.1016/j.jsames.2012.01.003

Melchor RN, Casadío S (2000) Hoja 3766-III La Reforma. Programa Nacional de Cartas Geológicas 1:250.000, Provincia de La Pampa. Servicio Geológico Minero Argentino, Boletín 295:1–56

Melchor RN, Llambías EJ (2004) Hoja Geológica 3766-I, Santa Isabel, Provincia de La Pampa. Programa Nacional de Cartas Geológicas 1:250.000 Secretaría de Minería de la Nación, Servicio Geológico Minero Argentino, Boletín N° 344. Buenos Aires

Novello VF, Cruz FW, Vuille M, Stríkis NM, Edwards RL, Cheng H, Emerick S, de Paula MS, Li X, Barreto E, Karmann I, Santos RV (2017) A high-resolution history of the South American Monsoon from Last Glacial Maximum to the Holocene. Sci Rep 7:44267. https://doi.org/10.1038/srep44267

Ortlieb L, Macharé J (1993) Former El Niño events: records from western South America. Global Planet Change 7:181–202

Razik S, Chiessi CM, Romero OE, von Dobeneck T (2013) Interaction of the South American Monsoon System and the Southern Westerly Wind Belt during the last 14 kyr. Palaeogeogr Palaeoclimatol Palaeoecol 374:28–40. https://doi.org/10.1016/j.palaeo.2012.12.022

Tooth S (2000) Process, form and change in dryland rivers: a review of recent research. Earth Sci Rev 51:67–107

Tooth S, McCarthy TS (2007) Wetlands in drylands: geomorphological and sedimentological characteristics, with emphasis on examples from southern Africa. Prog Phys Geogr 31(1):3–41

Tooth S, Nanson GC (2011) Distinctiveness and diversity of arid zone river systems. In: Thomas DSG (ed) Arid zone geomorphology: process, form and change in drylands, 3º. Wiley-Blackwell, Chichester, pp 269–300

Tooth S, Ellery F, Grenfell M, Thomas A, Kotze D, Ralph T (2015a) 10 reasons why the Geomorphology of wetlands is important. Wetlands in Drylands Research Network. http://wetlandsindrylands.net/wp-content/uploads/2015a/10/10-Reasons-Geomorphology-of-Wetlands-NEAR-FINAL-PRINTER-FRIENDLY.pdf.

Tooth S, Grenfell M, Thomas A, Ellery W (2015b) Wetlands in Drylands: 'Hotspots' of Ecosystem Service Provision in Marginal Environments. Science Brief for the United Nation's Global Sustainable Development Report (GSDR)—2015b Edition. https://sustainabledevelopment.un.org/content/documents/640493-Tooth-Wetlands%20in%20Drylands_Hotspots%20of%20Ecosystem%20Services%20in%20Marginal%20Environments.pdf

Torres E, Zambrano J (2000) Hidrogeología de la Provincia de Mendoza. En: Argentina. Recursos y Problemas Ambientales de las Zonas Áridas. Primera Parte: Provincias de Mendoza, San Juan y La Rioja. Tomo I: Caracterización Ambiental

Tripaldi A, Forman SL (2007) Geomorphology and chronology of Late Quaternary dune fields of western Argentina. Palaeogeogr Palaeoclimatol Palaeoecol 251:300–320. https://doi.org/10.1016/j.palaeo.2007.04.007

Tripaldi A, Zárate M (2017) Geoformas eólicas de la cuenca del Río Salado-Chadileuvú, Provincia de La Pampa, Argentina. XX Congreso Geológico Argentino, San Miguel de Tucumán, Argentina

Tripaldi A, Zárate MA, Brook GA, Li GQ (2011) Late Quaternary paleoenvironments and paleoclimatic conditions in the distal Andean piedmont, southern Mendoza. Argentina Quat Res 76:253–263. https://doi.org/10.1016/j.yqres.2011.06.008

Tucker ME (2003) Sedimentary rocks in the field, 3rd ed. The Geological Field Guide Series. Chichester: Wiley

Universidad Nacional de La Pampa (Unlpam), Facultad Ciencias Exactas y Naturales (2012) Línea de base biótica, hidrológica y productiva. Estudio para la cuantificación monetaria del daño causado a la provincia de La Pampa por la carencia de un caudal fluvio ecológico del río Atuel. Volume II (2)

Urbiztondo AM (1974) Fotointerpretación del área de los ríos Salado y Atuel (con cartografía reducida) desde el paralelo 35º 45' al paralelo 38º a escala 1:50.000. Consejo Provincial del Agua de La Pampa. 21 pp. Santa Rosa. Unpublished.

Wittmann F, Householder E, de Oliveira WA, Lopes A, Junk WJ, Piedade MTF (2015) Implementation of the Ramsar Convention on South American wetlands: an update. Res Rep Biodivers Stud 4:47–58. https://doi.org/10.2147/RRBS.S64502

Zárate MA, Mehl A (2011) Evolución geomorfológica holocena de la cuenca media del río Atuel, Mendoza, Argentina. XVIII Congreso Geológico Argentino. Neuquén, Argentina

Zárate M, Urrutia J, Lanzillotta R, Mehl A (2005) Estudio para la determinación del caudal mínimo necesario para el restablecimiento del sistema ecológico fluvial en el curso inferior del río Atuel. Capítulo 6: características geomorfológicas y sedimento-pedológicas. Universidad Nacional de La Pampa

Zárate MA, Dornes PF, Mehl A, Tripaldi A, Lorenzo F (2018) Bañados del Atuel (provincia de La Pampa, Argentina): de humedal a desierto, ¿un camino sin retorno? VII Congreso Argentino de Cuaternario y Geomorfología. Puerto Madryn, Argentina. Abstracts book